Rheological properties of confined thin films

M. Schoen and S. Hess
Institut für Theoretische Physik, Technische Universität Berlin, Hardenbergstrasse 36, 10623 Berlin, Germany

D. J. Diestler
Department of Agronomy, University of Nebraska-Lincoln, Lincoln, Nebraska 68583-0915

(Received 1 May 1995)

Shearing of monolayer and bilayer monatomic films confined between planar solid surfaces (walls) is simulated by a Monte Carlo technique in the isostress-isostrain ensemble, where temperature, number of film atoms, and applied normal stress are state variables. The walls consist of individual atoms that are identical with the film atoms and are fixed in the fcc (face centered cubic) (100) configuration. The lattice constant l of the walls is varied so that the walls are either commensurate with the (solid) film at fixed nominal lattice constant l_f (i.e., $l/l_f=1$) or homogeneously compressed ($l/l_f<1$) or stretched ($l/l_f>1$). Such rheological properties as shear stress T_{zx} and modulus are correlated with molecular structure of the layers, as reflected in translational and orientational correlation functions. If the walls are properly aligned in transverse directions, then the layers exhibit a high degree of fcc order. As such ordered films are subjected to a shear strain (by reversibly moving the walls out of alignment), they respond initially as an elastic solid: at small strains, T_{zx} depends linearly on the strain. As the shear strain increases, the response becomes highly nonlinear: T_{zx} rises to a maximum (yield point) and then decays monotonically to zero, where the maximum misalignment of the walls occurs. The correlation functions indicate that the films are not necessarily solid, even when the walls are in proper alignment. The results suggest that the principal mechanism by which disordered nonsolid films are able to resist shearing is "pinning": the film atoms are trapped in effective cages formed by their near neighbors and the mutual attraction of the walls for the caged atoms pins them together.

PACS number(s): 61.20.Ja, 68.45.Nj

I. INTRODUCTION

A. Experimental background

The rheological behavior of thin films confined between planar solid surfaces has been under intensive study in recent years, spurred by the development of a host of scanning surface probe devices, in particular the atomic force microscope (AFM) [1–5] and the surface forces apparatus (SFA) [6–10], which allow the study of such films directly on the nano- and molecular scales. In essence the SFA comprises two plane parallel sheets (walls) of molecularly smooth mica sandwiching a thin film of the fluid of interest, typically a liquid under normal conditions. The sandwich is immersed in the bulk fluid, which is held at constant temperature and pressure. The film is *open* to the bulk fluid, which serves as a thermal and material reservoir. Thus, if thermodynamic equilibrium between the film and bulk is maintained, the temperature and chemical potential of the film are fixed. By electromechanical means the separation and alignment of the walls can be manipulated with nearly molecular precision.

In one mode of operation of the SFA, the normal stress T_{zz} on the walls is measured as a function of the distance between them. As the separation between the walls varies from 1 to about 10 mean molecular diameters, T_{zz} oscillates between attraction and repulsion, regardless of the nature of the fluid [11]. These oscillations have also been seen in theoretical treatments of model films by integral equation [12–14], density functional [15,16], Monte Carlo [17–21], and molecular dynamics [22–26] methods. Variations in the local density indicate that the fluid arranges itself in layers parallel with the walls and that as the distance between the walls increases (decreases) whole layers appear (disappear), more or less abruptly. In particular, grand canonical ensemble Monte Carlo (GCEMC) simulations [21] of what we shall henceforth refer to as the prototypal slit pore [i.e., a Lennard Jones (12,6) film confined between walls comprising like atoms rigidly fixed in the face-centered-cubic (100) configuration] show that solid films form by epitaxy even though the bulk state lies in the fluid region of the Lennard-Jones phase diagram. If the walls are in registry (see Fig. 1) then the film contains an odd number of solid layers, each having a distorted fcc (100) configuration; if the walls are out of registry, then the film has an even number of solid layers. The formation of solid layers is a direct consequence of the template effect, which can be apprehended by viewing the entire system (walls plus film) as part of a bulk fcc crystal. The (100) planes must be stacked, say along the z axis, in a repeating sequence, ...*abab*..., where the b planes are displaced with respect to the a planes in the x or y direction by $0.5l$, l being the lattice constant.

In another mode of operation of the SFA [27,28], the film is sheared by sliding the walls over one another at a fixed normal stress. The applied shear stress, T_{zx}, is mea-

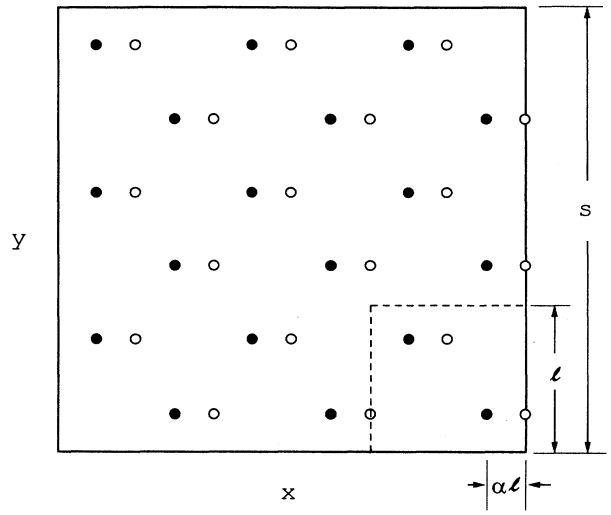

FIG. 1. Top view of slit pore. Filled circles represent atoms in wall (1) at $z=0$; open circles stand for atoms in wall (2) at $z=s_z$; l is the lattice constant associated with the fcc(100) plane. Walls are depicted with shear strain (registry) $\alpha \approx 0.25$.

sured as a function of the transverse alignment of the walls (i.e., the shear strain, or registry). When the walls are separated by only a few molecular diameters (i.e., by only a few layers), sliding cannot be initiated until a critical stress (the so-called yield stress of the film) is exceeded. The walls then slide over each other, eventually coming to rest, until the critical stress is once again attained and the walls again slip past each other. This stick-slip cycle, observed for all types of compounds ranging from long-chain (e.g., hexadecane) to spheroidal (e.g., OMCTS) hydrocarbons [10], has been attributed by Gee *et al.* [29] to the formation of a solidlike film that pins the walls together (region of sticking) and must be made to flow plastically in order for the walls to slip. This suggests that the structure of the walls induces the formation of a solid film when the walls are properly registered and that the film "melts" when the walls are moved out of the correct registry. Noting that the stick-slip phenomenon is general, in that it is observed in every liquid investigated, and that the yield stress may exhibit hysteresis, Granick [10] has argued that mere confinement may so slow mechanical relaxation of the film that flow must be activated on a time scale comparable with the experiment.

B. Theoretical background

Shear melting of solid vicinal films was first investigated theoretically by means of the GCEMC method applied to the prototypal slit pore [30]. Use of the GCEMC method is justified on the ground that in most realistic circumstances sliding in the SFA occurs at very low speed on a molecular scale. Thus, in the simulations we represent sliding as a quasistatic process, that is, as a succession of equilibrium states, each being specified by the registry α, which is the quantitative measure in terms of the fcc lattice constant of the relative transverse displacement of the walls (see Fig. 1). The chemical potential μ, temperature T, and separation of the walls s_z are also fixed. It is found that the solid films behave elastically up to a critical registry α_c, where almost an entire layer of the film drains from the pore, leaving behind loosely packed fluidlike layers that continue to sustain a nonnegligible shear stress. The strength of the solid film, reflected in the shear modulus $\partial T_{zx}/\partial(\alpha l)$, decreases with the number of layers, whereas the critical registry increases and the critical stress decreases.

Under certain conditions drainage seems not to occur in the SFA [27]. To simulate this situation, it is convenient to adopt an isostress-isostrain ensemble, in which the number N of film molecules is fixed along with T, T_{zz}, and the remaining (complementary) strains, except the registry. Using a nonequilibrium molecular dynamics (MD) technique based on this ensemble, Thompson and Robbins [31] examined the dynamic effects of shearing a monolayer film in the prototype with fcc (111) walls. They found that below a critical relative transverse speed of the walls, a freeze-flaw cycle like that seen in the earlier GCEMC simulation of quasistatic shearing [30] establishes itself. Above this critical speed the film molecules do not have time to form the epitaxial structure. It is interesting to speculate whether additional order not related to the structure of the walls can be dynamically induced by shearing. Nonequilibrium MD simulations [32–36] have shown that in homogeneous simple dense fluids under shear tubules of hexagonally close-packed strings of molecules form parallel with the streamlines. Presumably, similar shear-induced structures would form in confined films, even between smooth (structureless) walls.

In an attempt to make a direct contact with the SFA, Lupkowski and van Swol [37] applied a hybrid simulation technique to the prototype in the grand-isostress ensemble, where μ, T, and T_{zz} are fixed parameters. They meld the GCEMC technique with the nonequilibrium isostress-isostrain molecular dynamics method to study drainage dynamically, finding again a periodic stick-slip transverse movement of the walls accompanied by a corresponding drainage-imbibition sequence.

C. Prior studies of monolayer films

A series of recent articles [38–40] has been devoted to the curious "shear-melting" transition of monolayer prototypal films. Quasistatic shearing at fixed load leads to behavior rather different from that at fixed s_z. At $\alpha=0$, where the walls are precisely in registry, the film is a fcc (100) layer under zero shear stress. As α increases, T_{zx} begins to rise linearly, as expected for an elastic solid. In-plane pair-correlation functions $g^{(2)}$ for states in this linear regime agree closely with the theoretical $g^{(2)}$ for a strained fcc (100) layer. As α increases beyond the linear range, T_{zx} goes through a maximum (i.e., the yield stress) and then decays monotonously, which suggests a phase change. Indeed, over distances encompassing several nearest neighbors $g^{(2)}$'s for states in the nonlinear regime resemble the $g^{(2)}$ for the corresponding bulk state. Nevertheless, that the film supports a substantial shear stress indicates the vicinal phase is not a normal fluid.

Shear melting is a continuous transition, in contrast to thermally induced melting at constant normal stress, which is first order. The enthalpy and the density are both continuous functions of α and fluctuation-related properties in the isostress-isostrain ensemble, such as isostress heat capacity, isothermal compressibility, and isostress expansivity, all diverge according to the power law $(\alpha-\alpha_c)^{\nu}$, where $\nu<0$, as α approaches the shear-melting point α_c [39]. This suggests that the transition is second order [41].

Another indication of the bizarre rheological character of the molten film is anomalous diffusion [40]. Using both (microcanonical) molecular dynamics and isostress-isostrain MC, we have computed the mean square displacement for states of the film above the shear-melting point α_c, where diffusion sets in on a time scale characteristic of molecular liquids. However, the diffusive process turns out to be non-Markovian (i.e., non-Brownian) in the vicinity of α_c. The mean square displacement exhibits a time dependence of the power-law form At^d, where d depends on α, varying between 0 for $\alpha<\alpha_c$, where the film is solid, and 1 at $\alpha=0.5$, where the film is fluidlike. The non-Brownian character of diffusion, which is indicative of a second-order transition [42], can be rationalized in terms of cooperative molecular motions in the highly constrictive microporous medium engendered by the potential field of the structured walls (see Fig. 2 of Ref. [40]).

Until now our attention has been restricted to solid monolayer films that are commensurate with the walls. Moreover, to reduce computational expense we have been using films with transverse dimensions just large enough so that computed (intensive) properties are independent of the interfacial area. This restriction, coupled with the requirement of periodic boundary conditions in transverse directions, limits the range over which $g^{(2)}$ can be determined to only about 4 atomic diameters. (If long-range translational correlations are present, they will be missed.) That the stick-slip phenomenon is observed [10] for ultrathin films of all sorts of fluids, regardless of the relationship between the molecular structure of the corresponding bulk phase and that of the mica sheets, indicates that simple epitaxy cannot explain stick-slip transverse motion in all circumstances. We therefore turn our attention here to the behavior of prototypal films not commensurate with the walls.

In Sec. II we describe the prototypal model quantitatively. Section III is devoted to the thermodynamic and statistical mechanical treatments, including the derivation of molecular expansions for the rheological and structural properties of the film. To delineate the film structure more fully than in previous work, we look at orientational order as well as translational order, as measured by the in-plane pair-correlation function $g^{(2)}$. Because of the template effect, we expect to see fourfold orientational order in the layers of the film. It therefore seems reasonable to monitor the shear-induced transition quantitatively in terms of the mean local fourfold order in a layer (O_4) and the fourfold correlations (g_4) within the layers. Likewise, if layers become fluidlike, yet still localized in the normal (z) dimension, we may expect to see sixfold (O_6 and g_6) order reminiscent of a two-dimensional film [43,44].

In Sec. IV we compare results for monolayers and bilayers that are both commensurate and incommensurate with the walls. By examining films that are either stretched or compressed homogeneously (in transverse dimensions) with respect to the walls, we attempt either to increase or to decrease the relative influence of film-wall forces. Variations of T_{zx} with α are correlated with variations of O_n and g_n ($n=4,6$). To separate the effects of film-film interactions entirely from film-wall interactions, we also examine shearing of an "ideal gas," whose molecules by definition are subject to only the potential field due to the walls. Section V presents the conclusions of this study and discusses implications for stick-slip behavior in more general circumstances.

II. DESCRIPTION OF THE MODEL

The model system is schematized quantitatively in Fig. 1. The walls are taken to be square, of side length s. Each wall comprises n_s^2 unit cells of side length equal to the fcc lattice constant l. Thus $s=n_s l$ and each wall contains $N_s=2n_s^2$ rigidly fixed atoms at areal density $d_s=N_s/s^2=2/l^2$. The coordinate system is so chosen that the edges of the walls are parallel with the x and y axes (Fig. 1). The lower wall (denoted by 1 and lying in the plane $z=0$) is fixed in this coordinate frame; the upper wall (denoted by 2 and contained in the plane $z=s_z$) can be moved transversely *only* in the x direction. The coordinates of the atoms in the two walls are therefore related by

$$\begin{aligned} x_j^{(2)}&=x_j^{(1)}+\alpha l\ , \\ y_j^{(2)}&=y_j^{(1)}\ , \\ z_j^{(2)}&=z_j^{(1)}+s_z=s_z,\quad j=1,2,3,\ldots,N_s\ . \end{aligned} \tag{1}$$

If $\alpha=0$, the walls are exactly in registry; if $\alpha=0.5$, they are exactly out of registry. In Fig. 1, they are depicted in an intermediate registry. Alternatively, we may regard α as the shear-strain parameter: $\alpha l z/s_z$ is the shear strain in the x direction in planes parallel with the walls.

The film, which is confined between the walls and constitutes the *system,* in the thermodynamic sense, consists of N mobile atoms governed by the total potential (configurational) energy

$$U=U_{FF}+U_{FS}^{(1)}+U_{FS}^{(2)}\ , \tag{2}$$

where each term is given by a pairwise sum of Lennard-Jones (12,6) interatomic potentials

$$u(r)=4\epsilon[(\sigma/r)^{12}-(\sigma/r)^{6}]\ , \tag{3}$$

where ϵ is the depth of the attractive well and σ is the effective diameter of the hard core. The contribution from film-film interactions is

$$U_{FF}=\tfrac{1}{2}\sum_{i=1}^{N}\sum_{j\neq i}^{N}u(r_{ij})\ , \tag{4}$$

and that from film-wall interactions is

$$U_{FS}^{(k)}=\sum_{i=1}^{N}\sum_{j=i}^{N_s}u(r_{ij}),\quad k=1,2\ , \tag{5}$$

where $r_{ij}=|\mathbf{r}_i-\mathbf{r}_j|$ and the superscripts k refer to the walls. To prevent film atoms from escaping through the walls, we add to U a hard-wall background potential. Periodic boundary conditions are applied in the x and y directions to eliminate edge effects. Hence, the system is supposed to be of infinite extent in the transverse directions.

For purposes of comparison we present results for the "ideal-gas" film, which is subject only to fluid-wall interactions:

$$U_{\rm id}=\sum_{k=1}^{2}U_{FS}^{(k)}\ . \tag{6}$$

In case the film is commensurate with the walls, $N=N_s$, the number of atoms in each wall, for the monolayer, or $N=2N_s$ for the bilayer. To construct films incommensurate with the walls, we fix the areal density of the film, $d_f=2/l_f^2$ (where l_f is the fcc lattice constant of the solid film), equal to the areal density of the walls in the commensurate case and vary the areal density of the walls, $d_s=2/l^2$. To maintain periodic boundary conditions, we set $n_s l=n_f l_f$. The ratio of the lattice constants, $l/l_f=n_f/n_s$, is therefore a ratio of integers.

III. STATISTICAL THERMODYNAMIC TREATMENT

A. Thermodynamics

The extensive variables describing the thermodynamic state of the film are the entropy S, the amount (number of film atoms) N, the interfacial area $A=s^2$, the distance between the walls s_z and the registry, or shear strain, α. In addition, of course, the thermodynamic state depends implicitly on the potential parameters ϵ and σ and upon the areal density d_s of the walls. Gibb's fundamental relation governing reversible transformations of the film can be expressed [45]

$$dU=TdS+\mu dN+\gamma' dA+T_{zz}Ads_z+T_{zx}Ad(\alpha l)\ , \tag{7}$$

where T is the absolute temperature, μ is the chemical potential, T_{zz} is the normal stress, T_{zx} is the shear stress, and

$$\gamma'=(T_{xx}+T_{yy})s_z/2 \tag{8}$$

is an interfacial tension. The quantities T_{xx} and T_{yy} are the stresses applied to the plane surfaces bounding the film in the x and y directions.

We can derive the mechanical-work terms in Eq. (7) starting with the standard expression

$$dW=-\sum_{\alpha}\sum_{\beta}T_{\alpha\beta}Vd(\Sigma_{\alpha\beta}) \tag{9}$$

from the continuum theory of solids [46–49]. In Eq. (9) V is the volume, $T_{\alpha\beta}$ and $\Sigma_{\alpha\beta}$ are elements of the stress and displacement-gradient tensors, respectively, and the sums on α and β run over the Cartesian components. In the case of the confined film, $V=s^2s_z$ and the only nonzero displacements are the three compressions ($d\Sigma_{xx}=ds/s$, $d\Sigma_{yy}=ds/s$, and $d\Sigma_{zz}=ds_z/s_z$) and one shear [$d\Sigma_{zx}=d(\alpha l)/s_z$], where the constraint of square walls, $s_x=s_y=s$, has been enforced. Substituting these expressions for V and $\Sigma_{\alpha\beta}$ into Eq. (9), we obtain

$$\begin{aligned}dW&=-[ss_zT_{xx}ds+ss_zT_{yy}ds\\&\quad+s^2T_{zz}ds_z+s^2T_{zx}d(\alpha l)]\\&=-[\gamma' dA+T_{zz}Ads_z+T_{zx}Ad(\alpha l)]\ ,\end{aligned} \tag{10}$$

where the third line of Eq. (10) is seen to be precisely the expression for the work appearing in Eq. (7).

Since the state variables that we wish to control are T and T_{zz}, rather than S and s_z, it is convenient to transform the internal energy U via

$$\hat{G}=U-TS-As_zT_{zz}\ , \tag{11}$$

where $\hat{G}$ is a kind of Gibbs potential analogous to $G=U-TS+pV$ for the homogeneous phase. Combining Eqs. (7) and (11), we obtain

$$d\hat{G}=-SdT+\mu dN+\gamma dA-As_zdT_{zz}+T_{zx}Ad(\alpha l)\ , \tag{12}$$

where

$$\gamma=\gamma'-T_{zz}s_z=\tfrac{1}{2}(T_{xx}+T_{yy}-2T_{zz})s_z \tag{13}$$

is the interfacial tension analogous to the ordinary liquid-vapor surface tension [50]. The Gibbs potential is regarded as a function of the independent state variables T, N, A, T_{zz}, and αl.

B. Statistical mechanics

A standard analysis following the approach of Schrödinger [51] and Hill [52] yields the expression

$$\hat{G}=-k_BT\ln D\ , \tag{14}$$

where k_B is Boltzmann's constant and the isostress-isostrain partition function D is given by

$$\begin{aligned}&D(T,N,A,T_{zz},\alpha l)\\&\quad=\sum_{s_z}\exp[As_zT_{zz}/k_BT]Q_N(T,A,s_z,\alpha l)\ .\end{aligned} \tag{15}$$

The canonical partition function Q_N is

$$Q_N=Z_N/\Lambda^{3N}N!\ , \tag{16}$$

where the configuration integral is given by

$$\begin{aligned}Z_N(T,A,s_z,\alpha l)&=\int_{V^N}d\mathbf{r}^N\exp[-U(\mathbf{r}^N;s_z,\alpha l)/k_BT]\\&=\prod_{j=1}\int_0^{s_z}dz_i\int_0^{s}dy_i\int_{\alpha lz_i/s_z}^{\alpha lz_i/s_z+s}dx_i\exp(-U/k_BT)\end{aligned} \tag{17}$$

and $\mathbf{r}^N$ represents the $3N$-dimensional configuration of the film and $d\mathbf{r}^N$ the corresponding volume element. The second line of Eq. (17) exhibits more fully the dependence of Z_N on the shear strain. The thermal de Broglie wavelength is defined by $\Lambda \equiv h(2\pi m k_B T)^{-1/2}$, where h is Planck's constant and m is the mass of a film atom.

C. Shear stress

The property of primary rheological interest in the current context of the shear stress T_{zx}, the formal expression for which follows from Eqs. (12), (14), and (15)

$$\begin{aligned} AT_{zx} &= [\partial \hat{G}/\partial(\alpha l)]_{T,N,A,T_{zz}} \\ &= -k_B T D^{-1}[\partial D/\partial(\alpha l)]_{T,N,A,T_{zz}} \\ &= -k_B T(\Lambda^{3N} N! D)^{-1} \sum_{s_z} \exp(As_z T_{zz}/k_B T)[\partial Z_N/\partial(\alpha l)]_{T,N,A} \ . \end{aligned} \tag{18}$$

Now depending upon how the partial derivative of Z_N is evaluated, Eq. (18) can yield two alternative expressions for T_{zx}. In the usual procedure one makes the change of variable

$$x_i' = x_i - \alpha l z_i / s_z \tag{19}$$

to recast Eq. (17) as

$$Z_N = \prod_{i=1}^{N} \int_0^{s_z} dz_i \int_0^{s} dy_i \int_0^{s} dx_i' \exp[-U\{x_i' + \alpha l z_i/s_z, y_i, z_i\}/k_B T] \ . \tag{20}$$

Differentiation of this expression with respect to (αl) leads, after considerable algebraic manipulation, to

$$-k_B T \partial Z_N/\partial(\alpha l) = s_z^{-1} \int_{V^N} d\mathbf{r}^N \exp[-U/k_B T] \left\{ \tfrac{1}{2} \sum_{i=1}^{N} \sum_{j \neq i}^{N} u'(r_{ij}) x_{ij} z_{ij}/r_{ij} + \sum_{k=1}^{2} \sum_{i=1}^{N} \sum_{j=1}^{N_s} u'(r_{ij}) x_{ij} z_{ij}/r_{ij} \right\} , \tag{21}$$

where $u' = du/dr$, $x_{ij} = x_i - x_j$, and so forth. Substituting Eq. (21) into Eq. (18), we have finally the "virial" expression

$$T_{zx} = T_{zx,ff} + T_{zx,fs} \ , \tag{22a}$$

where the film-film and film-wall contributions are given respectively by

$$T_{zx,ff} = \tfrac{1}{2} A^{-1} \sum_{i=1}^{N} \sum_{j \neq i}^{N} \langle u' x_{ij} z_{ij}/r_{ij} s_z \rangle \ , \tag{22b}$$

$$T_{zx,fs} = A^{-1} \sum_{k=1}^{2} \sum_{i=1}^{N} \sum_{j=1}^{N_s} \langle u' x_{ij} z_{ij}/r_{ij} s_z \rangle \tag{22c}$$

and the angular brackets signify the isostress-isostrain ensemble average. By definition, the isostress-isostrain ensemble average of a general property $G(\mathbf{r}^N; s_z)$ is given by

$$\langle G \rangle = \sum_{s_z} \int_{V^N} d\mathbf{r}^N P(\mathbf{r}^N; s_z) G(\mathbf{r}^N; s_z) \ , \tag{23}$$

where the isostress-isostrain distribution function is defined by [38]

$$P(\mathbf{r}^N; s_z) = \frac{\exp[(As_z T_{zz} - U(\mathbf{r}^N))/k_B T]}{\sum_{s_z} \int_{V^N} d\mathbf{r}^N \exp\{[As_z T_{zz} - U(\mathbf{r}^N)]/k_B T\}} \ . \tag{24}$$

The alternative expression for T_{zx} is obtained by direct differentiation of Z_N given in the second line of Eq. (17). Application of Leibniz's rule [53] produces

$$\begin{aligned} -k_B T \partial Z_N/\partial(\alpha l) &= \prod_{i=1}^{N} \int_0^{s_z} dz_i \int_0^{s} dy_i \int_{\alpha l z_i/s_z}^{\alpha l z_i/s_z + s} dx_i \exp[-U/k_B T] \partial U_{FS}^{(2)}/\partial(\alpha l) \\ &= \prod_{i=1}^{N} \int_0^{s_z} dz_i \int_0^{s} dy_i \int_{\alpha l z_i/s_z}^{\alpha l z_i/s_z + s} dx_i \exp[-U/k_B T] \sum_{i=1}^{N} \sum_{j=1}^{N_s} u'(r_{ij}) \partial r_{ij}/\partial(\alpha l) \ , \end{aligned} \tag{25}$$

where the contributions from the upper and lower limits of the integration on x_i cancel each other on account of the periodic boundary conditions. In Eq. (25) r_{ij}, which refers to the distance between the ith film atom and the jth atom in the upper wall, is given by

$$\begin{aligned} r_{ij}^2 &= [x_i - x_j^{(2)}]^2 + [y_i - y_j^{(2)}]^2 + [z_i - z_j^{(2)}]^2 \\ &= [x_i - (x_j^{(1)} + \alpha l)]^2 + [y_i - y_j^{(1)}]^2 + [z_i - s_z]^2 \ , \end{aligned} \tag{26}$$

where the second line follows from Eq. (1). Using Eq. (26), we readily compute

$$\partial r_{ij}/\partial(\alpha l) = -x_{ij}/r_{ij} \ . \tag{27}$$

Substituting Eqs. (25) and (27) into (18) and simplifying the result, we obtain

$$T_{zx} = -A^{-1}\sum_{i=1}^{N}\sum_{j=1}^{N_s}\langle u' x_{ij}/r_{ij}\rangle \ . \tag{28}$$

The right member of Eq. (28) is clearly the *negative* of the mean value of the x component of the force $F_x^{(2)}$ (divided by the area A of the wall) exerted by the film on the upper wall (2), or equivalently the average x component of the force (per unit area) exerted by the upper wall on the film. Thus we have

$$\begin{aligned} -F_x^{(2)} &= -\left\langle \sum_{i=1}^{N} \partial U_{FS}^{(2)}/\partial x_i \right\rangle \\ &= AT_{zx} = -\sum_{i=1}^{N}\sum_{j=1}^{N_s}\langle u' x_{ij}/r_{ij}\rangle \\ &= \langle \partial U_{FS}^{(2)}/\partial(\alpha l)\rangle \ . \end{aligned} \tag{29}$$

By symmetry, of course, T_{zx} is the mean x component of the force $F_x^{(1)}$ (divided by A) acting on the lower wall (1).

Another useful rheological measure is the shear modulus defined by

$$\begin{aligned} c_{44} &\equiv \partial T_{zx}/\partial(\alpha l) \\ &= A^{-1}\partial[\langle \partial U_{FS}^{(2)}/\partial(\alpha l)\rangle]/\partial(\alpha l) \ , \end{aligned} \tag{30}$$

where the second line is due to Eq. (29). The shear modulus is the analog of one of the isothermal elastic stiffness constants used to characterize homogeneous solids [48]. For the confined film there are four strains: three compressions and one shear. The subscript 4 designates the shear strain, according to the notation in Ref. [38]. A nonzero value of the shear modulus clearly indicates a film capable of sustaining a shear stress and suggests a solid or glassy phase. Using Eqs. (23) and (24), we can rewrite Eq. (30) as

$$\begin{aligned} c_{44} &= A^{-1}\partial/\partial(\alpha l)\left\{\left[\sum_{s_z}\exp(As_z T_{zz}/k_B T)Z_N\right]^{-1}\sum_{s_z}\exp(As_z T_{zz}/k_B T)\int_{V^N} d\mathbf{r}^N \exp(-U/k_B T)\partial U_{FS}^{(2)}/\partial(\alpha l)\right\} \\ &= A^{-1}((k_B T)^{-1}\{\langle \partial U_{FS}^{(2)}/\partial(\alpha l)\rangle^2 - \langle[\partial U_{FS}^{(2)}/\partial(\alpha l)]^2\rangle\} + \langle \partial^2 U_{FS}^{(2)}/\partial(\alpha l)^2\rangle) \ . \end{aligned} \tag{31}$$

The indicated partial derivatives required in Eq. (31) are given in terms of the intermolecular potential by

$$\begin{aligned} \partial U_{FS}^{(2)}/\partial(\alpha l) &= -\sum_{i=1}^{N}\sum_{j=1}^{N_s} u'(r_{ij})x_{ij}/r_{ij} \ , \\ \partial^2 U_{FS}^{(2)}/\partial(\alpha l)^2 &= \sum_{i=1}^{N}\sum_{j=1}^{N_s}\{u'' x_{ij}^2/r_{ij}^2 + u'/r_{ij} - u' x_{ij}^2/r_{ij}^3\} \ . \end{aligned} \tag{32}$$

D. Molecular structure

The instantaneous number density operator $\rho(\mathbf{r})$, given by

$$\rho(\mathbf{r}) = \sum_{i=1}^{N}\delta(\mathbf{r}_i - \mathbf{r}) \tag{33}$$

where δ is the Dirac delta function, can be employed to characterize the film's molecular structure in part. The mean value of ρ is given by

$$\begin{aligned} \langle\rho(\mathbf{r})\rangle &= \sum_{i=1}^{N}\sum_{s_z}\prod_{k=1}^{N}\int_V d\mathbf{r}_k P(\mathbf{r}^N; s_z)\delta(\mathbf{r}_i - \mathbf{r}) \\ &= \sum_{i=1}^{N}\sum_{s_z}\prod_{k\neq 1}^{N}\int_V d\mathbf{r}_k P(\mathbf{r}_1, \mathbf{r}_2, \ldots, \mathbf{r}_i = \mathbf{r}, \ldots, \mathbf{r}_N; s_z) \\ &= \sum_{i=1}^{N} P^{(1)}(\mathbf{r}_i = \mathbf{r}) \ , \end{aligned} \tag{34}$$

where $P^{(1)}(\mathbf{r}_i = \mathbf{r})$ is the probability of atom i being at $\mathbf{r}$, regardless of the positions of the other atoms. Since the atoms are equivalent, $P^{(1)}$ is independent of i and the summation on i in Eq. (34) can be performed explicitly to yield

$$\langle\rho(\mathbf{r}_1)\rangle = NP^{(1)}(\mathbf{r}_1) = \rho^{(1)}(\mathbf{r}_1) \ . \tag{35}$$

In general, $\rho^{(1)}(\mathbf{r}_1)$ is a function of the *vector* position of the point of observation $\mathbf{r}_1$. However, since we are concerned mainly with the inhomogeneity of the film in the normal (z) direction, the average of $\rho^{(1)}(\mathbf{r}_1)$ over the interfacial area is adequate. This yields

$$\rho^{(1)}(z)=A^{-1}\int_0^s dx_1\int_0^s dy_1\rho^{(1)}(\mathbf{r}_1)\ , \tag{36}$$

to which we shall henceforth refer simply as the local density. In essence we regard the film as if it were cylindrically symmetric. In practice the local density is determined by partitioning the range $0<z<s_z$ into imaginary layers of width Δz, and ensemble averaging the number of atoms in each layer.

The molecular structure of the layers in transverse directions is partially revealed by correlations in the number density operator, given by

$$\begin{aligned}\langle\rho(\mathbf{r})\rho(\mathbf{r}')\rangle&=\sum_{i=1}^{N}\langle\delta(\mathbf{r}_i-\mathbf{r})\delta(\mathbf{r}_i-\mathbf{r}')\rangle+\sum_{i=1}^{N}\sum_{j\neq i}^{N}\langle\delta(\mathbf{r}_i-\mathbf{r})\delta(\mathbf{r}_j-\mathbf{r}')\rangle\\&=\rho^{(1)}(\mathbf{r})\delta(\mathbf{r}-\mathbf{r}')+\sum_{i=1}^{N}\sum_{j\neq i}^{N}\sum_{s_z}\prod_{k\neq i,j}\int_V d\mathbf{r}_k P(\mathbf{r}_1,\mathbf{r}_2,\ldots,\mathbf{r}_i=\mathbf{r},\ldots,\mathbf{r}_j=\mathbf{r}',\ldots,\mathbf{r}_N;s_z)\ ,\end{aligned} \tag{37}$$

where the "self-term" gives no new information beyond the mean density. Again invoking the equivalence of films atoms, we recognize the cross term in Eq. (37) as the pair distribution function

$$\rho^{(2)}(\mathbf{r}_1,\mathbf{r}_2)=N(N-1)P^{(2)}(\mathbf{r}_1,\mathbf{r}_2) \tag{38}$$

which is related to the mean density through the pair-correlation function by

$$\rho^{(2)}(\mathbf{r}_1,\mathbf{r}_2)=\rho^{(1)}(\mathbf{r}_1)\rho^{(1)}(\mathbf{r}_2)g^{(2)}(\mathbf{r}_1,\mathbf{r}_2)\ . \tag{39}$$

In general, $g^{(2)}$ is a six-dimensional function of the positions of reference (x_1,y_1,z_1) and observed (x_2,y_2,z_2) atoms. However, to be consistent with the approximation of cylindrical symmetry for the local density we take $g^{(2)}$ to be a function only of the normal coordinate (z_1) of the reference atom and the cylindrical coordinates ρ_{12} and z_{12} of the observed atom relative to the reference atom. (ρ_{12} and z_{12} are, respectively, the magnitudes of the projection of r_{12} onto the x-y plane and the z axis. That is, $\mathbf{r}_{12}=\boldsymbol{\rho}_{12}+z_{12}\hat{e}_z$, where $\hat{e}_z$ is the unit vector in the z direction.) Moreover, to simplify further the description of the transverse structure, we consider only the "in-plane" pair-correlation function, where $z_2=z_1$:

$$g^{(2)}\sim g^{(2)}(z_1,\rho_{12},z_{12}=0)\ . \tag{40}$$

Because the layers are in practice extremely well localized, we assign an in-plane pair-correlation function $g^{(2)}$ to each layer. The ith layer is bounded in the normal direction by imaginary planes that intersect the nearest relative minima in $\rho^{(1)}$ on either side of the relative maximum (z_i) near the center of the layer. $g^{(2)}$ is a function only of ρ_{12} and is computed from the formula

$$g^{(2)}(\rho_{12})=\langle N(\rho_{12})\rangle/2\pi\rho_{12}\Delta\rho_{12}\Delta z_{12}\rho^{(1)}(z_i)\ , \tag{41}$$

where $\langle N(\rho_{12})\rangle$ is the mean number of atoms in an annulus of radius ρ_{12}, width $\Delta\rho_{12}$, and height Δz_{12} centered on the reference atom 1, and $\rho^{(1)}(z_i)$ is the *mean* local density of the ith layer, which is determined by averaging the local density over the layer:

$$\rho^{(1)}(z_i)=\Delta z_{12}^{-1}\int_{z_i-\Delta z_{12}/2}^{z_i+\Delta z_{12}/2}dz\,\rho^{(1)}(z)\ . \tag{42}$$

Additional insight into the transverse structure of the layers is afforded by the in-plane orientational density operator

$$\rho_n(\mathbf{r})=\sum_{j=1}^{N}\delta(\mathbf{r}_j-\mathbf{r})\psi_n(\mathbf{r}_j)\ , \tag{43}$$

where

$$\psi_n(\mathbf{r}_j)=n^{-1}\sum_{i=1}^{n}\exp(in\theta_{ij}) \tag{44}$$

is the complex n-fold orientational order parameter associated with atom j [44,54]. The sum on i in Eq. (44) runs over the n nearest neighbors of j that lie in the same layer and

$$\theta_{ij}=\cos^{-1}[\boldsymbol{\rho}_{ij}\cdot\hat{e}_x/\rho_{ij}] \tag{45}$$

is the angle between the x axis and the projection of $\mathbf{r}_{ij}=\mathbf{r}_i-\mathbf{r}_j=\boldsymbol{\rho}_{ij}+z_{ij}\hat{e}_z$ onto the x-y plane.

The mean value of $\rho_n(\mathbf{r})$ is given by

$$\begin{aligned}\langle\rho_n(\mathbf{r})\rangle&=\sum_{i=1}^{N}\sum_{s_z}\prod_{k\neq i}^{N}\int_V d\mathbf{r}_k P(\mathbf{r}_1,\mathbf{r}_2,\ldots,\mathbf{r}_i=\mathbf{r},\ldots,\mathbf{r}_N;s_z)\psi_n(\mathbf{r}_1,\mathbf{r}_2,\ldots,\mathbf{r}_i=\mathbf{r},\ldots,\mathbf{r}_N)\\&=N\sum_{s_z}\int_V d\mathbf{r}_2\int_V d\mathbf{r}_3\cdots\int_V d\mathbf{r}_N P(\mathbf{r},\mathbf{r}_2,\mathbf{r}_3\cdots\mathbf{r}_N;s_z)\psi_n(\mathbf{r},\mathbf{r}_2,\mathbf{r}_3\cdots\mathbf{r}_N)\ ,\end{aligned} \tag{46}$$

where the second line follows from the equivalence of film atoms. Although $\mathbf{r}$ in Eq. (46) is by definition restricted to a given layer, in general $\langle\rho_n(\mathbf{r})\rangle$ depends on $\mathbf{r}$. We can nevertheless obtain a rough measure of orientational order within the layer by averaging $\langle\rho_n(\mathbf{r})\rangle$ over the layer:

$$\begin{aligned}O_n(z_i)&=\int_0^s dx\int_0^s dy\int_{z_i-\Delta z_{12}/2}^{z_i+\Delta z_{12}/2}dz\langle\rho_n(\mathbf{r})\rangle/\rho^{(1)}(z_i)A\,\Delta z_{12}\\&=\int_0^s dx\int_0^s dy\int_{z_i-\Delta z_{12}/2}^{z_i+\Delta z_{12}/2}dz\langle\rho_n(\mathbf{r})\rangle/\langle N_i\rangle\ .\end{aligned} \tag{47}$$

Here $\langle N_i \rangle$ is the mean number of atoms in the ith layer. In practice the numerator on the right-hand side of Eq. (47) is computed by ensemble-averaging the quantity $\sum_{j=1}^{N_i}\psi_n(\mathbf{r}_j)$.

In analogy to $\rho^{(2)}(\mathbf{r},\mathbf{r}')$, cross correlations of the in-plane orientational density operator yield useful information about the range of the n-fold orientational order within layers of the film. The cross term in $\langle \rho_n^*(\mathbf{r})\rho_n(\mathbf{r}') \rangle$ is given by

$$C_n(\mathbf{r},\mathbf{r}')=N(N-1)\int_V d\mathbf{r}_3\int_V d\mathbf{r}_4\cdots\int_V d\mathbf{r}_N P(\mathbf{r},\mathbf{r}',\mathbf{r}_3,\mathbf{r}_4,\ldots,\mathbf{r}_N;s_z) \times\psi_n^*(\mathbf{r},\mathbf{r}',\mathbf{r}_3,\mathbf{r}_4,\ldots,\mathbf{r}_N)\psi_n(\mathbf{r}',\mathbf{r},\mathbf{r}_3,\mathbf{r}_4,\ldots,\mathbf{r}_N)\ , \tag{48}$$

where $\mathbf{r}$ and $\mathbf{r}'$ are restricted to a given layer i and the equivalence of film atoms has again been invoked. Consistent with our approximation that the in-plane $g^{(2)}$ depends only on ρ_{12}, we now take C_n to be a function only of ρ_{12}. We then define a reduced in-plane orientational correlation function by

$$g_n(\rho_{12})=\frac{\int_0^s dx\int_0^s dy\int_{z_i-\Delta z_{12}/2}^{z_i+\Delta z_{12}/2}dz\int_0^{2\pi}d\phi\int_{-\Delta z_{12}/2}^{\Delta z_{12}/2}dz_{12}C_n(\mathbf{r}_1,\mathbf{r}_2)\rho_{12}\Delta\rho_{12}}{A\,\Delta z_{12}[\rho^{(1)}(z_i)]^2[2\pi\rho_{12}\Delta\rho_{12}\Delta z_{12}g^{(2)}(\rho_{12})]}\ . \tag{49}$$

In practice the numerator of Eq. (49) is evaluated as an ensemble average of the sum $\sum_k\sum_{j\neq k}\psi_n^*(\mathbf{r}_k)\psi_n(\mathbf{r}_j)$ over all pairs (k,j) in layer i for which atoms k and j are separated by $\rho_{12}\pm\Delta\rho_{12}/2$; the denominator is just the number of such pairs.

Within the framework of our approximation that the film is homogeneous and isotropic in transverse dimensions, C_n is real. First note that $C_n^*(\mathbf{r}_1,\mathbf{r}_2)=C_n(\mathbf{r}_2,\mathbf{r}_1)$, which follows from Eq. (48) and the invariance of $P(\mathbf{r}_1,\mathbf{r}_2,\ldots,\mathbf{r}_N)$ under interchange of any two identical atoms. Second, since C_n depends only on ρ_{12}, it is likewise invariant upon interchange of $\mathbf{r}_1$ and $\mathbf{r}_2$. Therefore, we have $C_n(\mathbf{r}_1,\mathbf{r}_2)=C_n(\mathbf{r}_2,\mathbf{r}_1)$. Combining the latter equality with the immediately preceding one yields $C_n^*=C_n$.

E. Isostress-isostrain Monte Carlo method

To compute ensemble averages $\langle G \rangle$ via Eq. (23), we employ the isostress-isostrain ensemble Monte Carlo technique by which (a numerical representation of) a Markov chain of configurations is generated according to the isostress-isostrain ensemble probability density $P(\mathbf{r}_N;s_z)$, given formally in Eq. (24). As detailed in Ref. [38], the chain is realized by a sequence of two consecutive stochastic events: diffusion of film atoms and homogeneous compression or dilation of the film in the normal dimension. Since s_z remains fixed during the diffusion step, the classical Metropolis algorithm [55] is used to determine whether the attempted displacement of an atom is accepted on the basis of the associated change in

TABLE I. Parameters of the system and the isostress-isostrain Monte Carlo procedure. See also Ref. [57]. All quantities are dimensionless.

Temperature, T^*	1.00
Normal stress, T_{zz}^*	0.00
Areal density of the film, d_f^*	0.782 72
Lattice constant, l^*	1.5985
Side length of film, $s^*(l/l_f)$	23.9775(15/16) 25.5760(16/15,16/16) 17.5835(11/12) 19.1820(12/12)
Starting configuration	fcc(100)
Number of equilibration steps	$(1.5-2.5)\times10^5$
Number of steps between computations of cumulative averages	$4N$
Total number of MC steps	$(4-30)\times10^6$
Side length of displacement cube	0.05−0.13
Radius of spherical primary zone	1.8
Thickness of cylindrical annulus of secondary zone	0.7
Radius of neighbor list	2.7
Potential cutoff	3.5
Displacement of wall, δs_z^*	0.1−0.15
Thickness of imaginary layer used in computation of $\rho^{(1)}$, Δz^*	0.01
Thickness of cylindrical annulus used in computation of correlation functions, $\Delta\rho_{12}^*$	0.02

the configurational energy, ΔU. To compute ΔU, we expand the configurational energy in a Taylor series of powers of the coordinate of the displaced atom, *after* displacing the atom. This reduces the computational work by 20–40 % over the conventional scheme [56,57].

After N diffusive steps, the film is subjected to compression or dilation in the z direction, which is accomplished by changing s_z by a small amount δs_z. The magnitude of δs_z is adjusted during a given run so that 60–70 % of the attempts are accepted. The film is compressed (or dilated) homogeneously, that is, the z coordinates of all film and wall atoms are scaled by the ratio of wall separations s_z *before* and *after* compression (dilation). Again ΔU needs to be computed to determine whether an attempted compression (dilation) is accepted. Since only the z component of the atom-atom separation r_{ij} is affected, it is convenient to store the in-plane projection ρ_{ij} and recompute the configurational energy resulting from compression (dilation) using the stored ρ_{ij} and the scaled z_{ij}.

We handle shearing of the film as a quasistatic (i.e., reversible) process. The shear strain (registry) is initially fixed at $\alpha=0$ for the monolayer or at $\alpha=0.5$ for the bilayer, which are the only cases we shall consider. The N film atoms are then placed between the walls in a solidlike fcc (100) configuration. The Markov chain for the beginning registry is generated and relevant ensemble averages are evaluated according to the specifications enumerated in Table I, where the entries are given in terms of the customary dimensionless (starred) units: distance ($r^*=r/\sigma$) in units of σ, energy ($E^*=E/\epsilon$) in units of ϵ, and temperature ($T^*=k_BT/\epsilon$) in units of ϵ/k_B. α is then increased by a small amount (0.01 to 0.05), a new Markov chain initiated from the final configuration at the initial registry and the ensemble averages evaluated. This procedure is repeated until the entire range of α is covered. In this way, all properties are obtained as functions of α at fixed N, T, and T_{zz}. In all cases to be considered in this work, $T^*=1.00$ and $T_{zz}^*=0.0$.

IV. RESULTS OF MONTE CARLO SIMULATIONS

Our previous study [38] was restricted to a monolayer film between fcc(100) walls having lattice constant $l^*=1.5985$ or areal density $d_s^*=0.782\,72$, which corresponds to wall atoms fixed so that nearest-neighbor distance is $l^*/2^{1/2}=1.1303$, a little larger than the separation $r_m^*=2^{1/6}=1.12$ at which the Lennard-Jones (12,6) interatomic potential energy is minimum. In all cases considered in this article, we set the areal density of the film d_f^* to this value. We adjust the lattice constant of the walls, l, so that $l/l_f=n_f/n$, where n_f and n are integers. If $l/l_f=1$, the walls are commensurate with the film; if $l/l_f<1$, the walls are compressed; if $l/l_f>1$, the walls are stretched. We consider the following cases: (i) monolayer ($l/l_f=16/16$, 15/16, 16/15; (ii) bilayer ($l/l_f=11/11$, 12/11).

A. Shear stress

To check the reliability of the computed quantity of prime interest, T_{zx}, we compare values obtained from both the "virial" [Eq. (22)] and "force" [Eq. (28)] expressions. Results listed in Table II for monolayer and bilayer commensurate films reveal excellent agreement. It is perhaps noteworthy that for the bilayer, the film-film and film-wall interactions make roughly equal contributions to the "virial" result, whereas the film-wall interaction alone determines the "force" result. It should also be noted that all values of T_{zx} for the monolayer agree with previously computed [38] values for the smaller system ($n_s=5$) to better than 1%.

1. Commensurate films

The points listed in Table II, along with additional ones, are plotted in Figs. 2(c) and 3(b) to exhibit the dependence of T_{zx} on registry in greater detail. For the commensurate monolayer, as α increases from 0.0, T_{zx} rises from zero to a maximum (the yield point α_y), where

TABLE II. Comparison of shear stress T_{zx}^* computed by "virial" [Eq. (22)] and "force" [Eq. (28)] expressions.

System	α	Eq. (22) $T_{zx,ff}^*$	Eq. (22) $T_{zx,fs}^*$	Eq. (22) T_{zx}^*	Eq. (28) T_{zx}^*
monolayer	0.0	0.000	−0.003	−0.003	0.003
	0.1	0.062	1.511	1.573	1.576
	0.2	0.087	1.665	1.752	1.759
	0.3	0.051	0.882	0.933	0.934
	0.4	0.019	0.291	0.310	0.309
	0.5	0.005	0.005	0.012	0.019
bilayer	0.0	0.000	0.006	0.006	−0.002
	0.1	−0.020	−0.045	−0.065	−0.069
	0.2	−0.136	−0.230	−0.366	−0.370
	0.3	−0.530	−0.898	−1.428	−1.428
	0.4	−0.415	−0.723	−1.138	−1.136
	0.5	0.002	−0.008	−0.006	−0.002

the shear modulus c_{44} vanishes [see Eq. (30)]. For $\alpha > \alpha_y$, T_{zx} decays monotonously to zero at $\alpha = 0.5$. For the bilayer, T_{zx} behaves similarly as α *decreases* from $\alpha = 0.5$ to 0, except that T_{zx} is negative.

By symmetry T_{zx} is periodic in α of period 1 and must vanish at $\alpha = 0$ and 0.5. However, depending on how many layers make up the film, it is either stable (i.e,. Gibbs potential is minimum) or metastable at these special points. Commensurate films with odd numbers of solid layers are stable when the walls are in registry ($\alpha = 0, \pm 1, \pm 2, \ldots$) and metastable when the walls are exactly out of registry ($\alpha = \pm\frac{1}{2}, \pm\frac{3}{2}, \ldots$); films with even numbers of solid layers are stable at $\alpha = \pm\frac{1}{2}, \pm\frac{3}{2}, \ldots$, and metastable at $\alpha = 0, \pm 1, \pm 2, \ldots$. Hence, to effect a positive displacement of the upper wall confining a monolayer at $\alpha = 0$, we must apply a positive force to the wall. This is true for all registries in the range $0 < \alpha < 0.5$. At $\alpha = 0.5$, the monolayer is metastable; a slight displacement must be opposed by a force in the opposite direction in order to keep the wall in place. That is, $T_{zx} < 0$ in the range $0.5 < \alpha < 1.0$. On the other hand, the bilayer is stable at $\alpha = 0.5$. A negative shear stress must be applied to move the upper wall toward $\alpha = 0.0$, where the film becomes metastable. In other words, the Gibbs potential is minimum at the registry of stability ($\alpha = 0, \pm 1, \pm 2, \ldots$ for the monolayer and $\alpha = \pm\frac{1}{2}, \pm\frac{3}{2}, \ldots$ for the bilayer).

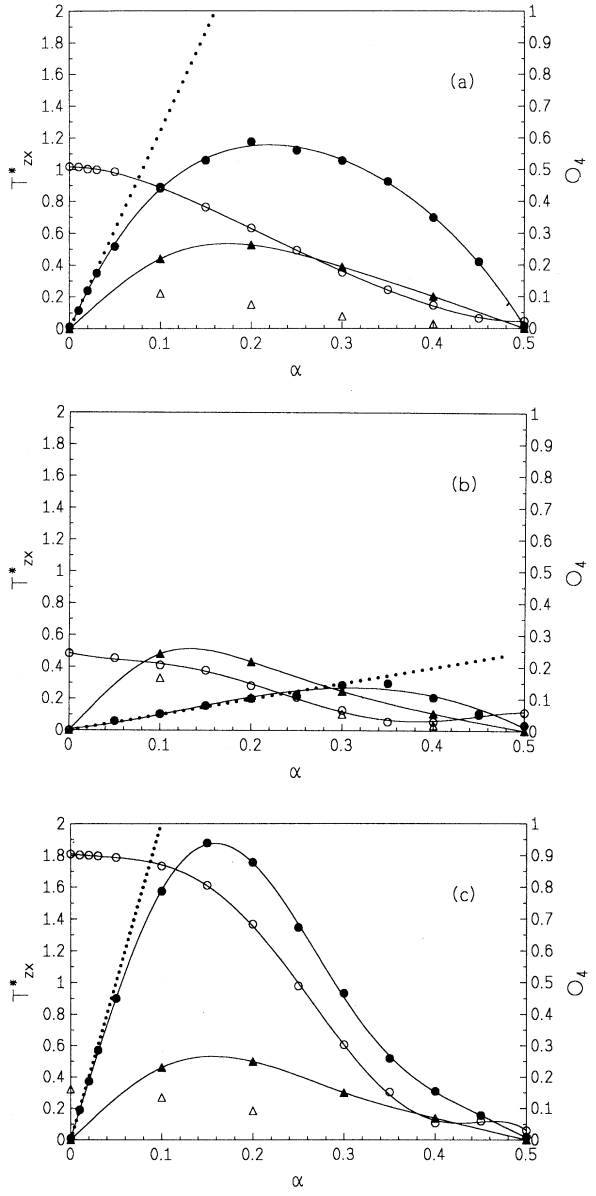

FIG. 2. Shear stress T^*_{zx}(●) and mean fourfold orientation (○) vs registry α for monolayers. (a) $l/l_f = 15/16$; (b) $l/l_f = 16/15$; (c) $l/l_f = 16/16$. Triangles (▲,△) refer to corresponding "ideal-gas" quantities. Solid lines are intended only to guide the eye.

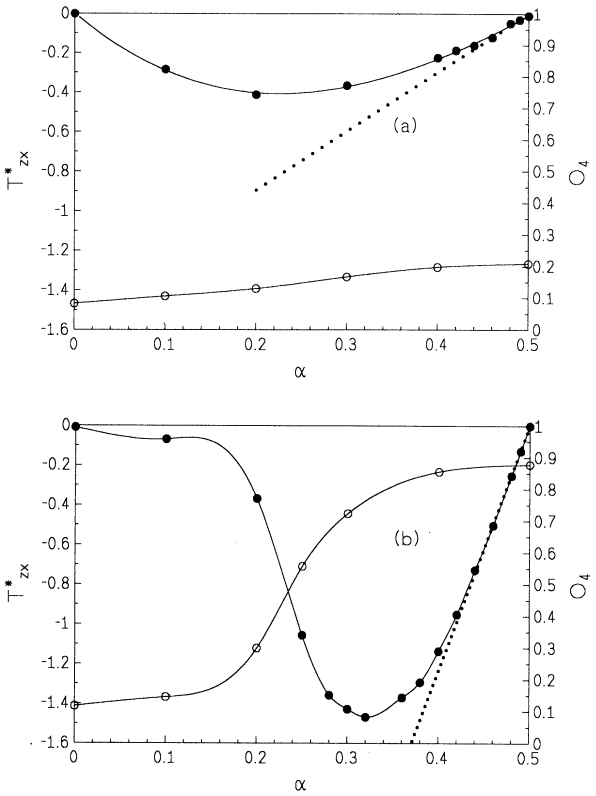

FIG. 3. Same as Fig. 2, except for bilayers. (a) $l/l_f = 11/12$; (b) $l/l_f = 11/11$.

The existence of a yield point signifies the film behaves nonlinearly. As α departs from the registry of stability the film becomes less elastic, eventually deforming plastically. We expect this to be reflected in the film's structure as a decrease in order, which we discuss in Sec. IV B. However, in the limit that the departure of α from the registry of stability is small, elastic behavior is observed. In this regime, the shear stress can be represented as

$$\begin{aligned} T_{zx} &\sim c_{44}^0 \alpha l \quad \text{(monolayer)}, \\ T_{zx} &\sim c_{44}^0 (\alpha - 0.5) l \quad \text{(bilayer)}, \end{aligned} \tag{50}$$

where c_{44}^0, the shear modulus of the stable solid film, is

computed from the expression in Eq. (31). Shear moduli, listed in Table III, are used in Eq. (50) to determine straight lines tangent to the shear stress curves at $\alpha=0$ or 0.5 (see Figs. 2 and 3). These plots demonstrate the reliability of c_{44}^0, but, more significantly, they also reveal substantial deviations from Hookean behavior at rather small displacements. The plastic regime begins already at $\alpha>0.03$ for the monolayer and $\alpha<0.44$ for the bilayer. The monolayer is stiffer than the bilayer, that is, c_{44}^0 for the monolayer is much greater than c_{44}^0 for the bilayer. Note that the yield point for the monolayer is displaced ($\Delta\alpha\sim0.15$) slightly less from the registry of stability ($\alpha=0$) than is the yield point for the bilayer ($\alpha\sim0.5-0.32=0.18$), although the yield stress supported by the monolayer is substantially greater. This is consistent with earlier results for the shearing of a multiple-layer solid film at fixed s_z, rather than fixed T_{zz} [30] and can be rationalized by a similar argument: as the number of layers in the film increases, the solidlike character of the layers decreases toward the center of the film and it takes less force to break down the less ordered structure of the inner layers.

2. *Incommensurate films*

Referring now to Figs. 2(a) and 3(a) and to Table III, we observe that the monolayer and bilayer between incommensurate walls compressed with respect to the film exhibit the following common characteristics: the yield point is shifted further from the registry of stability, the yield stress is lower, and the film is less stiff than for the commensurate counterpart. The shifts are relatively greater for the bilayer than for the monolayer. This is perhaps not surprising, since the template effect is expected to be weaker for the more compressed wall confining the bilayer.

As can be seen in Fig. 2(b), stretching the walls slightly (6.66%) has a much stronger influence on the shearing behavior of the monolayer than does compressing them by a comparable fraction (6.25%). The range of elasticity of the stretched-wall film appears to be extended appreciably, compared with films between commensurate or compressed walls.

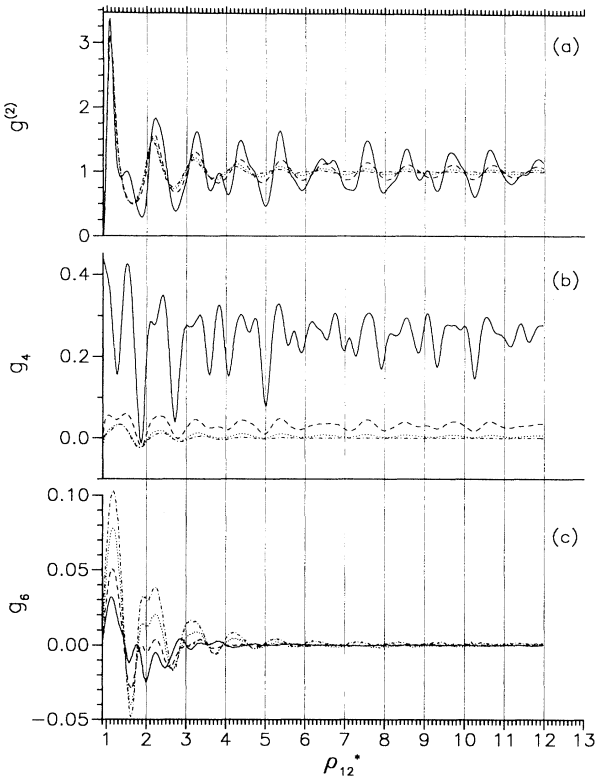

FIG. 4. Dependence of $g^{(2)}$, g_4, and g_6 on registry for the incommensurate ($l/l_f=15/16$) monolayer. $\alpha=0.0$, ——; $\alpha=0.3$, — — —; $\alpha=0.4$, · · · ·; $\alpha=0.5$, —·—·—· .

B. Molecular structural changes accompanying shearing

The connection between rheological behavior of the films and their molecular structure can be seen in the dependence of mean fourfold orientational order O_4 (Figs. 2 and 3) and of the translational and orientational correlations $g^{(2)}$, g_4, and g_6 (Figs. 4–8) on registry.

1. *Commensurate films*

From Eqs. (43), (44), and (47) we deduce that $O_4=1$ for a perfect fcc(100) lattice. But Figs. 2(c) and 3(c), respec-

TABLE III. Rheological characteristics of prototypal films. All quantities are dimensionless.

Film	l/l_f	α_y^a	$T_{zx}(\alpha_y)^*$	c_{44}^{0*}	$\langle s_z^* \rangle^b$
monolayer	16/16	0.15	1.88	12.6	1.689
	15/16	0.20	1.18	8.4	1.825
	16/15	0.35	0.30	0.6	1.961
bilayer	11/11	0.32	−1.47	7.7	2.532
	11/12	0.25	−0.47	2.0	2.843
"ideal gas"	16/16	0.16	0.50	5.4	1.862
	15/16	0.17	0.50		1.901
	16/15	0.14	0.50		1.811

[a]Registry at yield point.
[b]At $\alpha=0.0$ for monolayer, $\alpha=0.5$ for bilayer.

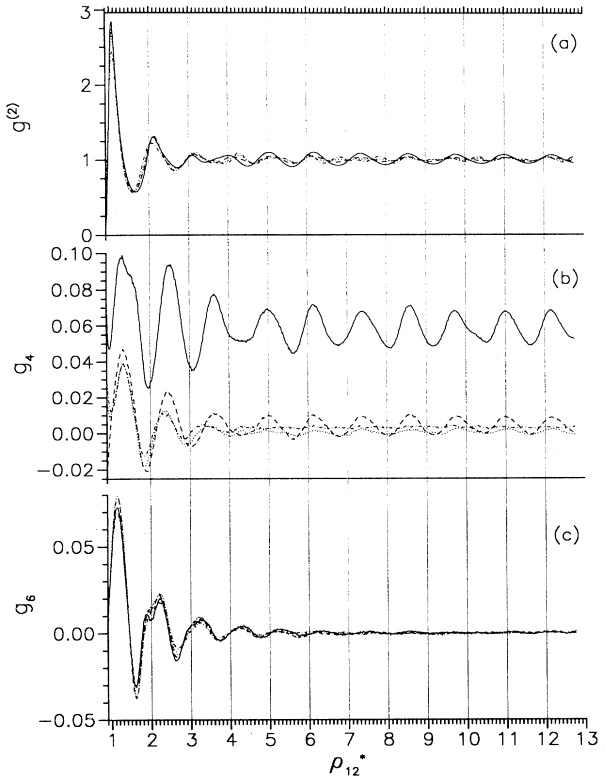

FIG. 5. Same as Fig. 4, except $l/l_f = 16/15$.

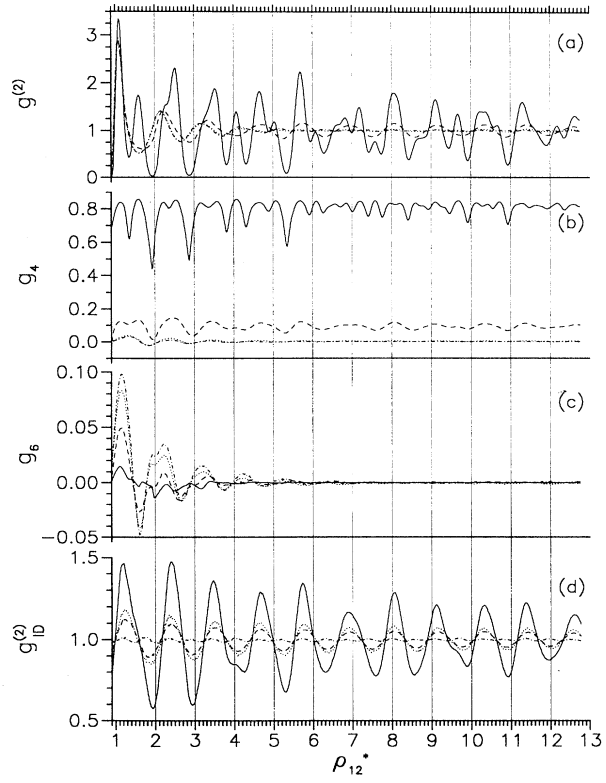

FIG. 6. Same as Fig. 4, except that film is commensurate with walls ($l/l_f = 16/16$). Panel (d) shows $g^{(2)}$ for the "ideal gas."

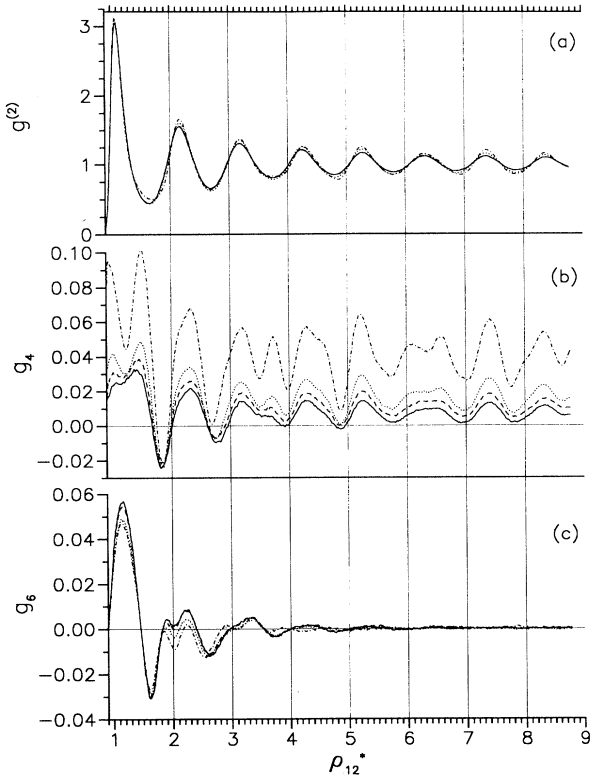

FIG. 7. Dependence of $g^{(2)}$, g_4, and g_6 on registry for the bilayer between compressed walls ($l/l_f = 11/12$). $\alpha = 0.0$, ——; $\alpha = 0.1$, — — —; $\alpha = 0.2$, · · · ·; $\alpha = 0.5$, —·—·— .

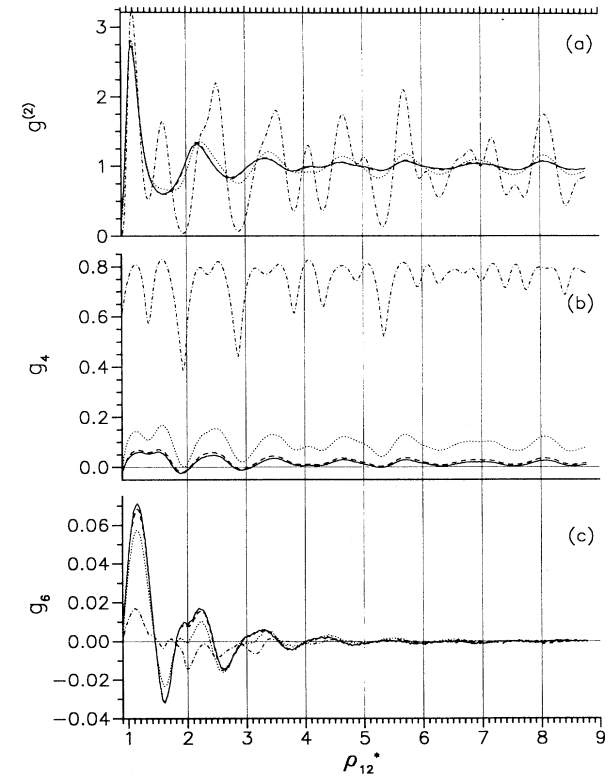

FIG. 8. Same as Fig. 7, except film is commensurate ($l/l_f = 11/11$) with walls.

tively, show that $O_4 \sim 0.9$ for the commensurate monolayer and bilayer. On account of thermal motion of the film, the film's layers are not perfectly ordered. Figures 6 and 8 also reflect the highly ordered state of the monolayer and bilayer films at their respective registries of stability, $\alpha=0$ and $\alpha=0.5$. In both cases $g^{(2)}$ virtually coincides with the theoretical $g^{(2)}$ for a (thermal) fcc(100) lattice, out to $\rho_{12}^* \sim 13$ for the monolayer and $\rho_{12}^* \sim 9$ for the bilayer. The corresponding g_4's confirm the strong fourfold coordination and the g_6's the lack of significant sixfold coordination indicative of a close-packed pseudo-two-dimensional layer [43,44]. At small strains, in the region of elastic behavior, O_4 remains nearly constant, reflecting the persistence of a solidlike film that responds harmonically to the applied stress. As the yield point is exceeded, O_4 declines rapidly, until the state of minimum order (the registry of metastability, which is $\alpha=0.5$ for monolayer and $\alpha=0.0$ for bilayer) is reached. The decrease in O_4 is mirrored in the correlation curves of Figs. 6 and 8, which indicate that the peaks decrease markedly in intensity and become smoother. Nevertheless, nonnegligible translational correlations clearly persist in $g^{(2)}$ and g_4 out to the limits $\rho_{12}^* \sim 12.8$ (monolayer) and $\rho_{12}^* = \rho_c^* \sim 9$ (bilayer) for registries well beyond [$\alpha \sim 0.3$ (monolayer), $\alpha \sim 0.2$ (bilayer)] the yield point. It is interesting that, even at their registries of metastability, both monolayer and bilayer retain a small degree of fourfold order, as seen in the nonzero values of O_4 in Figs. 2(c) and 3(b). It is particularly evident in the plot of g_4 for the bilayer [see Fig. 8(b)]. Note that for the bilayer g_4 remains long range at the registry of metastability, whereas for the monolayer g_4 becomes short range in this limit. As g_4 decreases, g_6 rises, although the latter drops off with ρ_{12} much faster than g_4, indicating that the sixfold coordination is short range.

The steady decline in O_4 with α for the monolayer [Fig. 2(c)] reflects a second-order transition, which is consistent with our earlier conclusion based on fluctuations in thermodynamic quantities [39] and on non-Brownian diffusion [40].

2. *Incommensurate films*

Plots of O_4 for monolayers and bilayers confined by compressed walls [see Figs. 2(a) and 3(a)] exhibit a dependence on registry like that of the commensurate films, except the magnitude and rate of decrease with departure of α from the registry of stability are smaller. This reflects softer and weaker films, as expected from the lessening of the template effect of the compressed walls.

The $g^{(2)}$ and g_4 for the monolayer between compressed walls (Fig. 4) display long-range correlations with the distinctive character of a strained fcc(100) layer, although the intensity of the correlations is uniformly lower. The peaks appear to be shifted inward compared with the commensurate case (Fig. 6). For example, the peak at $\rho_{12}^* = l^* \sim 1.6$ in Fig. 6(a) lies at $\rho_{12}^* = l^* \sim 1.5$ in Fig. 4(a), that is, the shift in the peak's position is approximately in proportion to the shift in the lattice constant of the wall. This suggests that a compressed solid monolayer forms epitaxially on compressed walls in registry. As α increases, fourfold coordination declines as sixfold rises; for registries beyond the yield point, the sixfold correlation becomes as strong as, or stronger than, fourfold, yet the latter appears longer range than the former, as for the commensurate monolayer.

In contrast to the monolayer, the bilayer between compressed walls shows $g^{(2)}$'s that vary only slightly with registry [Fig. 7(a)]. The same is true for the g_6's. It may be a mere curiosity that the structure of $g^{(2)}$'s for the compressed bilayer are very similar to that of $g^{(2)}$ for the compressed monolayer at $\alpha=0.3$ and that O_4 for the bilayer varies only slightly around 0.2, the value of O_4 for the monolayer near $\alpha \sim 0.3$. The structures of the g_4's are also similar. It should be emphasized that, although the monolayer between compressed walls clearly displays the features of a compressed solidlike fcc(100) film, the bilayer between compressed walls lacks any vestiges of the fcc structure. We presume the walls are too much compressed.

O_4 for the monolayer between stretched walls at $\alpha=0$ is less by a factor of about 2 than O_4 for the monolayer between compressed walls [see Fig. 2(b)]. Scrutinizing the plots creatively, one can descry the remnants of fcc(100) structure in $g^{(2)}$ and g_4 (Fig. 5), with peaks much reduced in magnitude and shifted to greater ρ_{12}^* compared with the commensurate monolayer. Short-range sixfold orientational correlation is, however, about as strong as fourfold and does not change appreciably as α varies. Note that fourfold correlations persist out to long distances ($\rho_{12}^* \sim 13$) even at the registry of metastability.

The compressed walls induce a compressed fcc(100) monolayer at $\alpha=0$, whereas the stretched walls cannot sustain a monolayer having clearly identifiable fcc character. From the last column of Table III, we note that the mean distance between the walls is greater for either incommensurate monolayer than for the commensurate one, which suggests that neither of the former fits as well between the walls as does the latter. Moreover, the stretched-wall monolayer fits less well than the compressed-wall one. The twelve near neighbors of each film atom (four in each wall and four in the film) conspire to cage the atom. If the walls are not too compressed, then the near-neighbors film atoms can move closer to form a tighter, albeit less stable, cage. All atoms are cooperatively caged to make up a compressed film. On the other hand, if the walls are stretched a little too much, the resulting cages are too loose to render the film truly solid. The phase has both solid and fluid character. How then does such a film support a shear stress?

C. "Ideal-gas" monolayers

To separate the effects of film-film and film-wall interactions on rheological behavior, we simulated the shearing of "ideal-gas" films, which neglect the film-film contribution to the potential energy [see Eq. (6)]. Plots of T_{zx} and O_4 are displayed in Fig. 2 and plots of $g^{(2)}$ in Fig. 6(d). The characteristic rheological parameters are listed in Table III. The similarity of the dependences of T_{zx} and O_4 on α among commensurate and incommensurate cases is striking. One should recall that the areal density

of film atoms is kept constant at $2/l_f^2$, while that of wall atoms varies according to $2/l^2$, where $l/l_f = n_f/n_s = 15/16$, $16/16$, and $16/15$. The film atoms do not "see" one another; they are free to arrange themselves independently in the field of the walls. They should therefore tend to be most populous in the minima, which for the commensurate case would be in the vicinity of the fcc(100) lattice points. We expect O_4 to be appreciable, as Fig. 2(c) indicates. Also, $g^{(2)}$ at $\alpha=0$ exhibits long-range correlation and peaks in one-to-one correspondence with those for the commensurate monolayer. Although the intensities of the peaks are much reduced, the relative magnitudes remain nearly the same, except that some sharp peaks in the commensurate case become barely perceptible shoulders in the "ideal-gas" plot.

We surmise that the gas atoms become localized in weak cages formed by the eight nearest neighbors in the walls. That is, the film atoms are localized in potential holes and their mutual attraction for each wall "pins" the walls. This pinning mechanism must of course play a role in the fully interacting film, for which the potential energy is given by Eq. (2). However, it is curious that film-film interactions appear to soften the film between stretched walls [see Fig. 2(b)]. The intermolecular forces apparently preclude the film atoms from adjusting their relative positions in order to fit nicely into the cages offered by the stretched walls. As discussed in Sec. IV B, this mismatch leads to a disorganized film, which consequently supports a smaller shear stress than the film between either commensurate or compressed walls.

V. DISCUSSION AND CONCLUSIONS

The original motivation for this work was a desire to clear up an apparent contradiction observed in earlier simulations [38] of shearing of prototypal commensurate monolayer films at constant T, N, and T_{zz}. The term "shear melting" was applied to the transition leading from a solid layer at $\alpha=0$, where $g^{(2)}$ displays features in precise correspondence to those of the fcc(100) plane, to a state where $g^{(2)}$ looks very similar to $g^{(2)}$ for fluidlike layers that are far removed from the walls in thick films [21], at least if one examines $g^{(2)}$ only as far as third near neighbors, which was the limit imposed by the size of the simulation cell [38]. Nevertheless, this fluidlike film is capable of sustaining a considerable shear stress. Here is the contradiction: to support a shear stress, the film would seem to need to possess a rigidity characteristic of solid and therefore to exhibit the long-range order of a solid.

The results of the present simulations indeed show that fourfold orientational order characteristic of the fcc(100) plane persists for values of α far beyond the yield point in the monolayer films between both commensurate and compressed walls. Sixfold order sets in gradually as α ranges from 0 to 0.5 and the fourfold order decreases. We surmise that this reflects the formation of a quasi-two-dimensional close-packed fluid.

The behavior of the monolayer between stretched walls is distinctly different from that of its counterpart between compressed walls. Although the former displays long-range fourfold orientational order, it is very much weaker. Moreover, the structures of $g^{(2)}$ and g_4 hardly bear a resemblance to the forms of $g^{(2)}$ and g_4 for the fcc(100) plane. With imagination one may argue that $g^{(2)}$ and g_4 for the stretched-wall case result from averaging out the fine fcc details clearly discernible in the plots for the compressed-wall counterpart. However, short-range sixfold order of the same magnitude as the fourfold order is present in the stretched-wall monolayer at all registries. This suggest that the state of the film is quasi-two-dimensional liquid with superposed weak long-range fcc order.

To separate the effects of film-film and film-wall interactions on the rheological properties of the monolayers, we examined the "ideal-gas" film, in which intermolecular forces among film atoms are set to zero, so that film atoms experience only the background potential of the rigid walls. The "ideal-gas" film does indeed support a substantial shear stress and also exhibits long-range translational and fourfold orientational order. The structure of $g^{(2)}$ for the commensurate case clearly displays averaged fcc(100) characteristics. We believe this to be due to the preferential occupation of the potential holes (or cages formed midway between the walls by the eight nearest neighbors about the hole) by the independent film molecules. The lattice of holes of course has fourfold symmetry identical with that of the fcc lattice. The less intense, "averaged" appearance of $g^{(2)}$ for the "ideal gas" is due to the lack of intermolecular forces among film molecules, which help to keep the molecules more localized in their potential holes in the case of the commensurate monolayer. That all "ideal-gas" films have about the same rheological parameters, regardless of the degree of commensurability of film and walls, reflects the freedom of the independent film atoms to adjust their positions without mutual interference in order to occupy the regular array of potential holes most efficiently.

The "ideal-gas" findings suggest that a primary mechanism by which monolayer films support an applied shear stress is "pinning:" the mutual attraction of the film molecules in their potential holes for each wall "pins" the walls. The (applied) "pinning" stress has a normal component T_{zz} and a transverse component T_{zx}. The latter vanishes when $\alpha=0$ or 0.5. Between these extremes of registry, the population of ideal gas molecules in the potential holes is distributed asymmetrically in the x direction, giving rise to a net stress opposing the applied shear stress.

We expect pinning to be enhanced with respect to the "ideal-gas" limit for commensurate films, since the forces on each molecule from its neighboring film molecules should assist the walls in keeping the molecule caged. On the other hand, intermolecular interactions within the film may actually weaken pinning, if the degree of incommensurability is large enough. Film-film interactions may not permit the film atoms to fit comfortably into cages. We pointed out in Sec. IV C how this happens for the monolayer between stretched walls.

The pinning mechanism is expected to operate in any monolayer film, regardless of the structure of the walls.

The key element is the existence of potential holes between relatively rigid walls that can be occupied by film molecules. Depending on the degree of commensurability of film and wall structures, the film will be more or less ordered. Pinning may therefore explain stick-slip behavior that is universally observed in SFA dynamic shear measurements of ultrathin liquid films [10]. This would assume, however, that the mica sheets are separated, in some regions at least, by only a monolayer.

Our results for the bilayer support that pinning also operates in thicker films. For example, the bilayer between compressed walls, for which long-range fourfold orientational order is evident, but extremely weak compared with that of its commensurate counterpart, is stiffer and stronger than the monolayer between stretched walls. Here pinning requires film-film interactions; with the walls far enough apart to accommodate a bilayer, their mutual attraction to the "ideal gas" would be negligible. The cooperation of both film-film and film-wall interactions results in the effective caging of film molecules. The cages are in general distorted from the fcc configuration; long-range order is accordingly reduced.

ACKNOWLEDGMENTS

D. J. Diestler is grateful for financial support of the U.S. Department of Energy under Grant No. DE-FG02/85ERGO310 and of the U.S. Army Research Office under Grant No. OAAL03-90-G-0074. M. Schoen is indebted to the Deutsche Forschungsgemeinschaft for financial support (Grant No. Scho 525/5-1). D. J. Diestler and M. Schoen are also thankful to the North Atlantic Treaty Organization for cooperative research Grant No. CRG 801927. The computations were performed on the Cray Y-MP/832 of the Höchstleistungrechenzentrum at Forschungszentrum Jülich. The authors are grateful to the Scientific Council of the HLRZ for a generous grant of computer time.

[1] G. Binnig, C. F. Quate, and Ch. Gerber, Phys. Rev. Lett. **56**, 930 (1986).
[2] C. M. Mate, G. M. McClelland, R. Erlandsson, and S. Chiang, Phys. Rev. Lett. **59**, 1942 (1987).
[3] R. Erlandsson, G. Hadziioannou, C. M. Mate, G. M. McClelland, and S. Chiang, J. Chem. Phys. **89**, 5190 (1989).
[4] E. Meyer, Prog. Surf. Sci. **41**, 3 (1992).
[5] M. B. Salmeron, MRS Bull. **18**, 20 (1993).
[6] D. Tabor and R. H. S. Winterton, Proc. R. Soc. London Ser. A **312**, 435 (1969).
[7] J. N. Israelachvili and D. Tabor, Proc. R. Soc. London Ser. A **331**, 19 (1973).
[8] J. N. Israelachvili and D. Tabor, Wear **24**, 386 (1973).
[9] J. N. Israelachvili and P. M. McGuiggan, Science **241**, 795 (1989).
[10] S. Granick, Science **253**, 1374 (1991).
[11] J. N. Israelachvili, Acc. Chem. Res. **20**, 415 (1987).
[12] D. Henderson, F. F. Abraham, and J. A. Barker, Mol. Phys. **31**, 1291 (1976).
[13] J. Fischer and M. Methfessel, Phys. Rev. A **22**, 2836 (1980).
[14] Y. Zhou and G. Stell, Mol. Phys. **66**, 767 (1989).
[15] B. K. Peterson, K. E. Gubbins, G. S. Heffelfinger, U. Marconi, and F. van Swol, J. Chem. Phys. **88**, 6487 (1988).
[16] E. Kierlik and M. L. Rosinberg, Phys. Rev. A **42**, 3382 (1990).
[17] J. E. Lane and T. H. Spurling, Aust. J. Chem. **29**, 2103 (1980).
[18] L. A. Rowley, D. Nicholson, and N. G. Parsonage, Mol. Phys. **31**, 365 (1976).
[19] F. F. Abraham, J. Chem. Phys. **68**, 3713 (1978).
[20] I. K. Snook and W. van Megen, J. Chem. Phys. **72**, 2907 (1980).
[21] M. Schoen, D. J. Diestler, and J. H. Cushman, J. Chem. Phys. **87**, 5464 (1987).
[22] S. Toxvaerd and E. Praestgaard, J. Chem. Phys. **67**, 5291 (1977).
[23] S. Toxvaerd, J. Chem. Phys. **74**, 1998 (1981).
[24] J. Q. Broughton and F. F. Abraham, Chem. Phys. Lett. **71**, 456 (1980).
[25] J. J. Magda, M. Tirrell, and H. T. Davis, J. Chem. Phys. **83**, 1888 (1985).
[26] M. Schoen, C. L. Rhykerd, Jr., J. H. Cushman, and D. J. Diestler, J. Chem. Phys. **88**, 1394 (1988).
[27] J. N. Israelachvili, P. M. McGuiggan, and A. M. Homola, Science **240**, 189 (1988).
[28] J. van Alsten and S. Granick, Phys. Rev. Lett. **61**, 2570 (1988).
[29] M. L. Gee, P. M. McGuiggan, J. N. Israelachvili, and A. M. Homola, J. Chem. Phys. **93**, 1895 (1990).
[30] M. Schoen, C. L. Rhykerd, Jr., D. J. Diestler, and J. H. Cushman, Science **245**, 1223 (1989).
[31] P. A. Thompson and M. O. Robbins, Science **250**, 792 (1990).
[32] J. P. Erpenbeck, Phys. Rev. Lett. **52**, 1333 (1984).
[33] S. Hess, Int. J. Thermophys. **6**, 657 (1985).
[34] L. V. Woodcock, Phys. Rev. Lett. **54**, 1513 (1985).
[35] W. Loose and S. Hess, Rheol. Acta **28**, 91 (1989).
[36] W. Loose and S. Hess, in *Microscopic Simulation of Complex Fluids,* edited by M. Mareschal (Plenum, New York, 1990), p. 267.
[37] M. Lupkowski and F. van Swol, J. Chem. Phys. **95**, 1995 (1991).
[38] M. Schoen, D. J. Diestler, and J. H. Cushman, Phys. Rev. B **47**, 5603 (1993).
[39] M. Schoen, D. J. Diestler, and J. H. Cushman, Mol. Phys. **78**, 1097 (1993).
[40] M. Schoen, J. H. Cushman, and D. J. Diestler, Mol. Phys. **81**, 475 (1994).
[41] H. E. Stanley, *Introduction to Phase Transitions and Critical Phenomena* (Clarendon, Oxford, 1971).
[42] J. Feder, *Fractals* (Plenum, New York, 1988).
[43] K. J. Naidoo, J. Schnitker, and J. D. Weeks, Mol. Phys. **80**, 1 (1993).
[44] T. Weider, M. A. Glaser, H. J. M. Hanley, and N. A. Clark, Phys. Rev. B **47**, 5622 (1993).
[45] D. J. Diestler, M. Schoen, J. E. Curry, and J. H. Cushman, J. Chem. Phys. **100**, 9140 (1994).
[46] L. D. Landau and E. M. Lifschitz, *Course of Theoretical*

Physics (Pergamon, Oxford, 1981), Vol. 7, Chap. 1.
[47] D. C. Wallace, *Thermodynamics of Crystals* (Wiley, New York, 1972), Chap. 2.
[48] H. Callen, *Thermodynamics* (Wiley, New York, 1966), Chap. 13.
[49] J. H. Weiner, *Statistical Mechanics of Elasticity* (Wiley, New York, 1983), Chap. 1.
[50] J. S. Rowlinson and B. Widom, *Molecular Theory of Capillarity* (Clarendon, Oxford, 1984).
[51] E. Schrödinger, *Statistical Thermodynamics* (Dover, New York, 1984), Chap. 2.
[52] T. L. Hill, *An Introduction to Statistical Thermodynamics* (Dover, New York, 1986), Chap. 1.
[53] H. Wayland, *Differential Equations Applied in Science and Engineering* (D. Van Nostrand, Lancaster, PA, 1964), p. 107.
[54] D. Frenkel and J. P. McTague, Phys. Rev. Lett. **42**, 1632 (1979).
[55] M. P. Allen and D. J. Tildesley, *Computer Simulation of Liquids* (Clarendon, Oxford, 1987).
[56] M. Schoen, D. J. Diestler, and J. H. Cushman, J. Chem. Phys. **101**, 6865 (1994).
[57] M. Schoen, J. Comput. Phys. **118**, 159 (1995).